Temporal thermal response of Type II–IR fiber Bragg gratings

Changrui Liao,[1] Dong-ning Wang,[1,*] Yuhua Li,[1] Tong Sun,[2] and Kenneth T. V. Grattan[2]

[1]Department of Electrical Engineering, The Hong Kong Polytechnic University, Hung Hom, Kowloon, Hong Kong, China

[2]School of Engineering and Mathematical Sciences, City University London, Northampton Square, London EC1V 0HB, U.K.

*Corresponding author: eednwang@polyu.edu.hk

Received 12 January 2009; revised 16 April 2009; accepted 26 April 2009; posted 29 April 2009 (Doc. ID 106284); published 22 May 2009

We use the phase mask method to investigate both experimentally and theoretically the temporal thermal response of Type II–IR fiber Bragg gratings inscribed by a femtosecond laser. A fast testing system is developed to measure the thermal response time by means of periodic CO_2 laser irradiation, which creates a rapid temperature change environment. The temporal thermal response is found to be independent of the heat power and the heat direction, although the grating produced destroys the axial symmetry of the fiber. The measured values of the temporal thermal response are ~230 ms for heating and ~275 ms for cooling, which different from the simulation results obtained from a lumped system equation. The causes of such differences are investigated in detail. © 2009 Optical Society of America

OCIS codes: 060.2340, 060.2370, 120.3940, 050.2770.

1. Introduction

A fiber Bragg grating (FBG) is one of the most widely used components in optical fiber sensors. In a high temperature sensor system that incorporates a FBG, the thermal stability and temporal thermal response are two of the most significant parameters that are reflected in the sensor performance. To improve the thermal stability of the FBG used extensively in a number of sensor systems, researchers have written gratings into carefully designed and fabricated special photosensitive optical fiber designed for use in high temperature measurement situations [1,2]. However, the cost of such special photosensitive fiber is high, limiting its widespread applicability. Recently, high power femtosecond laser pulses have been used to write FBGs in hydrogen-free fibers [3–6], and the Type II–IR gratings obtained with this method show excellent thermal stability, even at temperatures in excess of 1000 °C [3,7]. This represents a significant improvement when compared with that of conventional UV-induced gratings and is useful for a number of applications.

Generally speaking, the temperature change of most systems occurs much more slowly than does the Bragg wavelength shift of the grating, and hence there is no need to consider the temporal response of the Bragg wavelength shift. However, there are some rapidly changing, dynamic systems in which knowledge of the temporal thermal response of the sensing elements used is especially important, such as in internal combustion engines [8], where the sensing elements should have a fast response time to follow closely the rapid change in temperature of the system. Thus, an ideal temperature sensor should exhibit both high temperature stability and fast response time, commensurate with the dynamic temperature changes being measured.

The dominant mechanism for the inscription of Type II–IR gratings when using IR femtosecond laser pulses likely results from an ionization process, perhaps triggered by self-focusing [3], which differs from the mechanism for fabrication of gratings in hydrogenated photosensitive fiber using UV laser radiation. Thus, the grating structure of the Type II–IR

0003-6935/09/163001-07$15.00/0

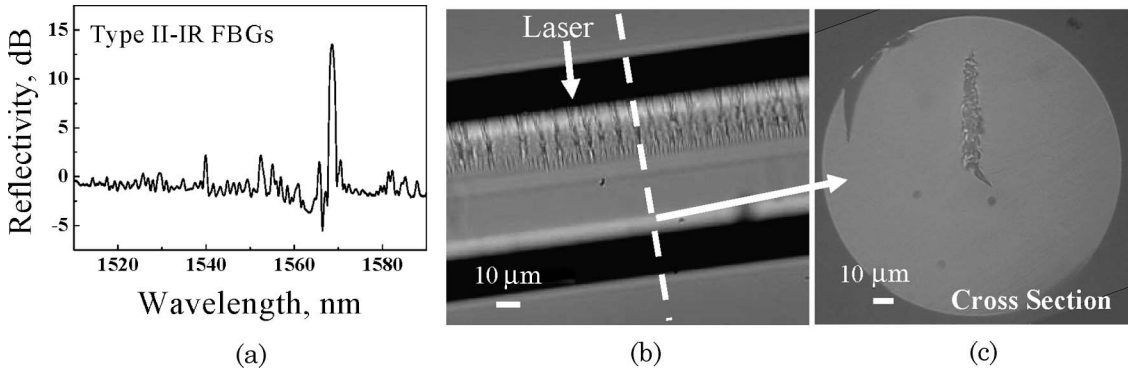

Fig. 1. Reflection spectrum and morphology of a Type II–IR FBG fabricated with a femtosecond laser by the phase mask method.

FBG not only exists in the fiber core but also extends to the cladding [3,9], which creates substantial axial asymmetry in the fiber cross section. Such asymmetry can reduce the directional uniformity of the FBG in any temperature sensing system created using them.

Here we investigate both experimentally and theoretically the temporal thermal response of Type II–IR FBGs inscribed by use of femtosecond laser pulses. In Section 2, the conditions to fabricate a Type II-IR FBG by use of femtosecond IR lasers through a phase mask are described and its reflection spectrum, morphology, and temperature sensitivity are presented. In Section 3, we discuss a simple setup that was built to investigate the temporal thermal response under different heating conditions, i.e., various heating powers and heating directions. In Section 4, we analyze the fiber heating and cooling under CO_2 laser irradiation using the lumped system, and the result of this simulation is compared with the measured data. Then the possible error sources are studied in detail. Finally, the results obtained in this work are discussed and the outcomes summarized in Section 5.

2. Characteristics of Type II–IR Fiber Bragg Gratings

The Type II–IR FBG investigated in this paper was fabricated based on a near field phase mask method. The inscription setup used is discussed in some detail in our previous paper [7]. The optical fiber used was a standard Corning SMF-28 fiber, used without hydrogen loading pretreatment. A Type II–IR FBG with reflectivity of ~13.2 dB was inscribed with a laser intensity of approximately $1.32 \times 10^{13}\,\mathrm{W/cm^2}$ and a 30 s exposure time. The length of the FBG was ~3 mm, limited by the laser beam size. There was no annealing process carried out for the grating after laser fabrication. The reflection spectrum and the morphology of the FBG are shown in Fig. 1. In the reflection spectrum, the obvious ripple seen is one of the typical features of a damaged grating. By observing the cross section, it is found that the groove resulting from severe femtosecond laser ablation goes beyond the core area so that the periodic refractive-index modulation is evident both in the core and in the cladding. This linear damage in the cladding destroyed the axial symmetry to the fiber axis that might become an influencing factor in the temperature sensing applications under consideration. Consequently, for a better understanding of the process, it is essential to study the relationship between the temporal response and the heating directionality.

Before the temporal response measurement, the calibration process was implemented to make sure there was a good correspondence between Bragg wavelength shift $\Delta\lambda_{\mathrm{Bragg}}$ and the temperature change that occurs in the tube furnace. To measure λ_{Bragg} most effectively and relate this as a function of temperature, the FBG was heated from room temperature of ~25 °C to 1150 °C, and the reflection spectrum was taken at each step after 10 min to allow for temperature stabilization. In the Grobnic *et al.* paper [10], the isothermal annealing behavior of femtosecond gratings showed a permanent wavelength drift at a temperature above 1000 °C, which might result in hysteresis in the wavelength response. In our case, however, the grating was heated at an ultrahigh temperature of >1000 °C for less than 30 min during the calibration process. Thus, the permanent wavelength drift induced could be neglected because of its low wavelength drift rate of several pm/h. The cycling heating experiment was implemented to eliminate errors in calibration. Figure 2 shows the variation of λ_{Bragg} as a function of temperature. The triangles on the graph represent the recorded data; the solid curve represents a quadratic fit to the data. Generally speaking, the optical fibers have two regions of different types of behavior: one for temperatures up to approximately 800 °C, where the Bragg wavelength shifts almost linearly with the increase in temperature; the other for the higher temperatures up to 1200 °C, where the Bragg wavelength shift has a nonlinear dependence on temperature that is due to the thermo-optic coefficient of fused silica glass [11]. The good quadratic relationship ($R^2 = 0.999$) indicates the high potential of the Type II–IR FBG in the ultrahigh temperature sensing applications investigated.

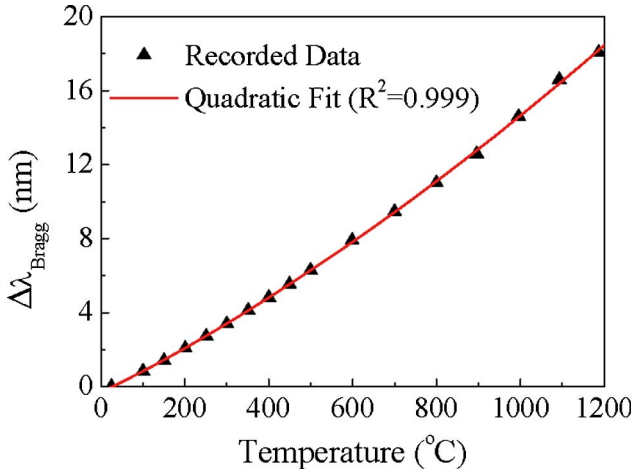

Fig. 2. (Color online) Graph showing the change of λ_{Bragg} as a function of temperature. The triangles represent the recorded data; the solid curve represents the quadratic fit.

3. Temporal Thermal Response of Type II–IR Fiber Bragg Gratings

A fast demodulation system is designed to investigate the temporal thermal response of a Type II–IR FBG to temperature heating and then cooling. The temporal thermal response as a function of laser heating directionality, arising due to the axial asymmetry of cross-sectional morphology, is discussed in Subsection 3.C.

A. Experimental Setup

Figure 3 shows the experimental setup used to measure the temporal thermal response of the FBG. Exposing the FBG to a step change in temperature was a challenge in the experiment. A CO_2 laser used in CW operation was chosen as the heat source because its output could be conveniently modulated by use of an optical chopper (3501, New Focus, San Jose, California) when heating and cooling the fiber. Another advantage of using a CO_2 laser was that the lasing wavelength was in the far infrared ($\lambda_{laser} = 10.6\,\mu m$) and the fused silica fiber absorbed almost all the incident laser energy [12]. The laser beam passed through a convex lens to broaden the beam diameter to irradiate the FBG more uniformly. A piece of plexiglass was irradiated by a CO_2 laser beam and the ablated region was observed to determine the intensity uniformity and the position of the beam. Then the position of the grating was precisely adjusted under continuous laser irradiation to obtain a drifted but still symmetric spectrum. Because chirping occurred as a result of the nonuniform distribution of the effective index of the guided mode, the spectrum broadened and became asymmetric [13].

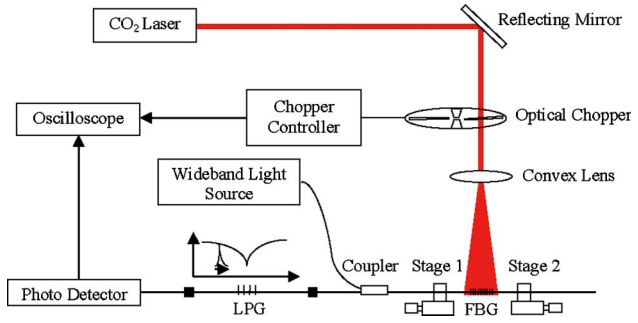

Fig. 3. (Color online) Experimental setup of the FBG used for temporal thermal response measurements.

To observe and record the fast signal change with the temperature, it is necessary to use a high speed demodulation system. To do so, a specified long period fiber grating (LPFG), acting as an edge filter, was connected to the tested FBG. Since λ_{Bragg} of the measured FBG in the room temperature region was around 1570 nm, the wavelength was expected to shift to 1575 nm under maximum irradiation; thus one LPFG was designed and fabricated with a linear falling edge profile at wavelengths between 1570 and 1575 nm in the transmission spectrum. As long as the FBG spectrum was shifted to longer wavelengths by heating with the CO_2 laser, the reflection wavelength signal of the FBG could be filtered along the falling edge of the LPFG, causing a change in the detector output power. Such a signal was easily recorded on the oscilloscope, as shown in Fig. 4. Because of the finite beam size that passed through the chopper, the laser power modulation was not an ideal rectangular waveform. The rise and fall times were calculated to be ~30 ms. The temporal response of this system overall is also dependent on the response characteristics of the photodetector used but overall it was designed to provide a sufficient demodulating speed for this application.

B. Heating and Cooling Experimental Results

The time constant is used to quantify the temporal thermal response, which is defined as the time for the temperature to change to $1 - 1/e$ or 63.2% of

Fig. 4. (Color online) Typical response of the detected optical power (lower trace) with the incident CO_2 laser signal (upper trace). Laser is ON at the rising edge of the signal and OFF at the constant high level. The upper trace refers only to the frequency reference output waveform from the chopper drive, not to the actual laser power. The laser power modulation has a rectangular waveform.

the difference between their initial and final temperatures during a sudden change in the surrounding temperature [14]. To study the time constant at different final temperatures, the FBG was heated by different laser powers. Because the laser power could not be adjusted in the CW operation, the incident power that irradiates the FBG was adjusted by changing the height of the FBG (the closer the FBG was to the convex lens, the higher the amount of laser power received). Experiments were implemented at three heights for the purpose of comparison, and the results obtained are demonstrated in the Fig. 5 inset. The beam diameter at each height was ~10, 8, and 5 mm, respectively, and we used Corning SMF-28e with a diameter of 125 μm. Thus the related dimensions of the beam to grating are around 220/1, 140/1, and 55/1, respectively. The spectrum drifts obtained at the three heights are also shown in Fig. 5. The calibration curve indicates that the final temperatures of the grating in the three cases are 330, 415, and 460 °C, respectively; the corresponding powers absorbed by the FBG are estimated to be 19, 24, and 27 mJ, respectively.

Figure 6 demonstrates the voltage signal recorded by the oscilloscope as a function of time at three different heating powers. To facilitate the observation, the voltage signal was reversed vertically before data analysis. The dots represent the recorded data; the solid curve represents the five-point smoothing of the data. When the heating power is increased by raising the FBG, the switching time increases (this is defined as the time for λ_{Bragg} to shift from its rest position to the point at which the photodetector voltage is at maximum). The switching time is another important parameter for applications such as temperature measurement because the final temperature will be known only after the switching time has elapsed. In Fig. 6, the switching time for the lower final temperature of 330 °C is ~750 ms, which is then increased to 780 ms for the medium level of

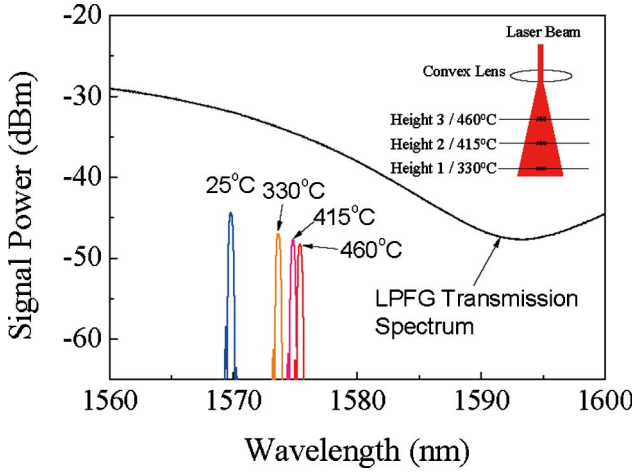

Fig. 5. (Color online) Spectrum of the LPFG superimposed with the FBG at room temperature, 330 °C, 415 °C, and 460 °C. Inset: relationship between the height of the FBG and the final temperature attained by the FBG.

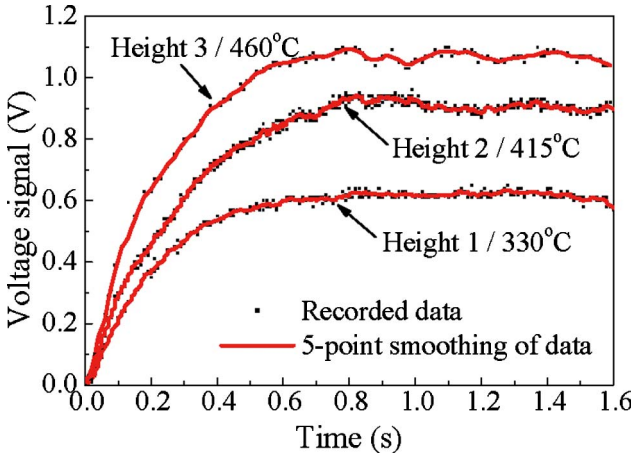

Fig. 6. (Color online) Heating curve as a function of time for a Type II–IR FBG, which is heated by a CO_2 laser beam at different heights, thus attaining different final temperatures.

415 °C. In the case of a higher final temperature of 460 °C, this value increases slightly to 790 ms. However, the temporal thermal response for heating the grating is found to be independent of the heating power and the final temperature. Thus the temporal thermal response of the heating system is measured to be 230 ± 25 ms.

The cooling was closely followed by the heating phase. Before the cooling started, the FBG should have reached a steady state, with the voltage signal being stable at a maximum for some time. When the CO_2 laser beam was shuttered (i.e., off), the FBG returned to room temperature quickly by dissipating the heat to the surrounding air. The reflection spectrum was shifted backward to its initial position, and the voltage signal fell to zero. Figure 7 shows the results of the FBG cooling, which was followed by the heating indicated in Fig. 6. The dots represent the recorded data; the solid curve represents the five-point smoothing of the data. Being similar to the result obtained in the heating, the switching time values for different initial temperatures are very close.

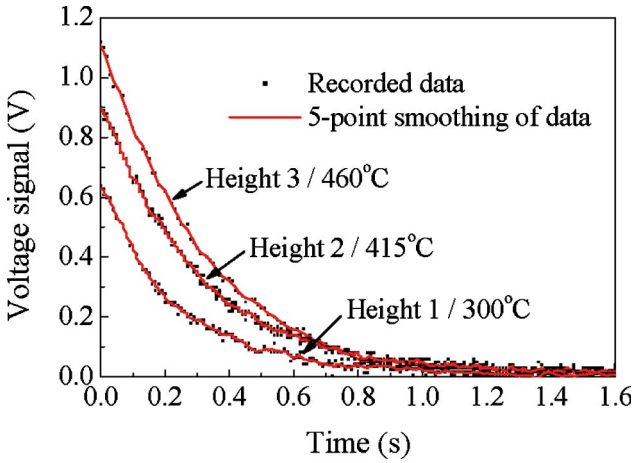

Fig. 7. (Color online) Cooling curves as a function of time of a Type II–IR FBG with different initial temperatures.

Corresponding to the different initial temperatures of 330, 415, and 460 °C, respectively, the switching times were measured to be nearly 1.34, 1.34, and 1.36 s, respectively. We also found that the temporal thermal response is independent of the initial temperature and was measured to be 275 ± 25 ms, which is slower than the value obtained for the heating phase.

C. Results of the Heating Directional Test

In the femtosecond laser-based phase mask inscription method, the axial symmetry of the fiber is destroyed, as has been discussed above. The refractive-index modulation is created in both the core and on one side of the cladding. To quantify the effect that is due to the axial asymmetry, the temporal thermal response was measured by rotating the FBG, in steps of 30°. The grating groove was parallel to the incident CO_2 laser at the beginning, as illustrated in the Fig. 8 inset, which shows the results of heating and cooling the fiber in terms of incident laser power from various directions. The triangles represent the measured data during laser heating; the squares represent the measured data from the cooling. By comparing the two curves, we found that the temporal thermal response is essentially independent of the fiber rotation (even though there was some slight fluctuation that might be induced by the change in the irradiation condition with fiber rotation). During the heating process, the measured temporal thermal response ranged from 200 to 250 ms, with an average value of 230 ± 25 ms. Similarly during the cooling, this same parameter ranged from 250 to 300 ms, and the average value was calculated to be 275 ± 25 ms. These results illustrate that the Type II–IR FBG has uniform temporal thermal response, which is essentially independent of the heating direction.

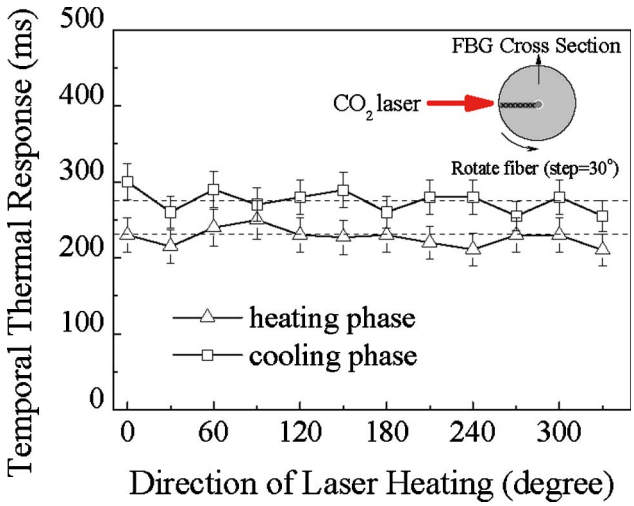

Fig. 8. (Color online) Temporal thermal response of a Type II–IR FBG as a function of the laser heating direction. The triangles represent the heating data; the squares represent the cooling data.

4. Theory of Fiber Heating and Cooling

Heating and cooling of a fiber resulting from periodic CO_2 laser irradiation can be described by a lumped system equation in a one-dimensional case [15,16]:

$$\frac{dT(t)}{dt} = -\frac{1}{\tau}(T(t) - T_{air}) + \Xi(t),$$
$$\tau = \frac{c\rho V_f}{A_f h} = \frac{c\rho r}{2h}, \Xi(t) = \frac{q(t)}{c\rho}, \quad (1)$$

with the initial condition

$$T(0) = T_{air}, \quad (2)$$

where $T(t)$ is the fiber temperature as a function of time, T_{air} is the temperature of the ambient air (300 K), c is the specific heat of the fiber (837 J kg^{-1} K^{-1}), ρ is the density of the fiber (2200 kg m^{-3}, V_f is the volume of the fiber, A_f is the surface of the fiber, h is the convection coefficient (400 W m^{-2} K^{-1}) [15], r is the radius of the fiber, $q(t)$ is the heat generation rate per unit volume, τ denotes the relaxation time, and $\Xi(t)$ represents periodic heating of the CO_2 laser beam.

The laser heating is expressed by use of an isosceles-trapezoid waveform with a rise and fall time of ~30 ms. The heating power within one period of ~4 s could be determined by the following equation:

$$\Xi(t) = \frac{k}{A_b r c \rho} P(t),$$
$$P(t) = \begin{cases} P_0 \frac{t}{30}, & 0 < t \le 30 \times \text{ms} \\ P_0, & 30\text{ms} < t \le 2000\text{ms} \\ P_0\left(-\frac{t}{30} + \frac{203}{3}\right), & 2000\text{ms} < t \le 2030\text{ms} \\ 0, & 2030\text{ms} < t \le 4000\text{ms} \end{cases}, \quad (3)$$

where $P(t)$ is the heating power as a function of time, P_0 is the incident heating power before encountering the chopper, k is the power absorption rate ($= 0.1\ \text{mm}^{-2}$), and A_b is the cross section of the laser beam (10).

For SMF-28 fiber ($r \approx 60\ \mu$m), assuming that the FBG is heated by a CO_2 laser at different powers, P_0 was set to 1, 0.7, and 0.5 W in Eq. (3). Through simulation results Fig. 9 shows that the temporal thermal response is independent of the heating power for both heating and cooling because the temporal thermal response is 160 ms for both the heating phase and the cooling phase. This value is somewhat different from the experimentally measured value but is in good agreement with the simulation result of ~140 ms in Ref. [15]. Sumetsky *et al.* [15] used an ideal rectangular waveform of heating power for the simulation without taking into consideration the rise and fall times of the power modulation. Therefore, there is a discrepancy of 20 ms when compared with our simulation results. In addition to the effect of the

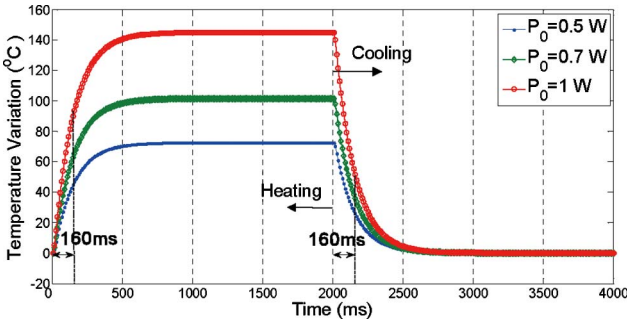

Fig. 9. (Color online) Simulated heating and cooling curves of a SMF-28 optical fiber heated at various laser powers.

rise and fall times, there are also other error sources that could affect the response measurement. First, the falling edge of the transmission spectrum of the LPFG is not perfectly linear but convex, thus the measured temporal response should be slightly longer than the actual value. Second, the CO_2 laser power fluctuation and the noise in the system would deteriorate the stability of the voltage signal on the oscilloscope, causing unavoidable measurement error. Due to the existence of these error sources, it is reasonable to explain the difference between the experimental measured value and the calculated value. However, we observed that our result is essentially consistent with others [12,15,17], all of which are in the range of $100–200 \times 10^{-3}$ s (within the range of experimental error). The differences result from the fiber used [12], the type of exposure [17], and other experimental conditions.

The effect of fiber size on the temporal thermal response has also been studied by use of this simulation, with the results shown in Fig. 10. Assuming an identical incident laser power ($P = 1$ W), the temporal thermal response of the fiber ($r = 30\,\mu$m) is measured to be 80 ms (heating phase) and 80 ms (cooling phase), which is significantly faster than the previous simulation result of 160 ms (heating and cooling phase) of the fiber with a radius of 60 μm. The results thus illustrate that the temporal thermal response is highly dependent on the fiber size (diameter), to be more accurate, the thermal mass of the fiber. As a result, an efficient method to enhance the temporal thermal response of the fiber sensors is to decrease the size of the optical fiber sensor itself,

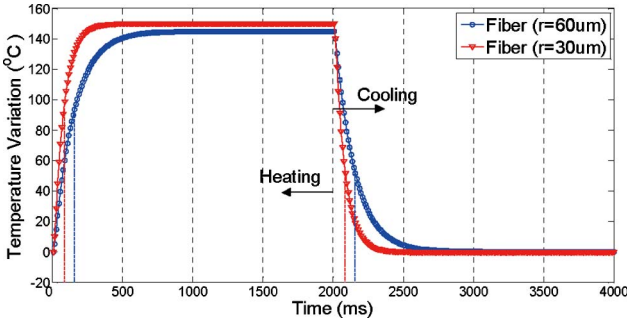

Fig. 10. (Color online) Simulated heating and cooling curves of two different size optical fibers at the same heating power.

which could be achieved by writing a FBG in an optical nanowire, for example. However, with the greatly reduced fiber size, the fiber sensor would become much more sensitive to temperature noise; therefore, the accuracy of temperature measurements would deteriorate. To strike a good balance between the temporal response and the temperature accuracy, the fiber size should be carefully designed based on what is necessary for practical measurement.

5. Conclusion

We have investigated the effect of optical heating on optical fibers that are used for optical fiber sensor systems. To do so we developed and used a fast testing system that incorporates periodic CO_2 laser irradiation for investigation of the temporal thermal response of Type II–IR FBGs, which have the potential to be used as high temperature sensors (>1000°C). Our experimental results show that the temporal thermal response of this grating is 230 ± 25 ms in the heating phase and 275 ± 25 ms in the cooling phase, which is independent of the heating power and the heating direction. The axial asymmetry in the fiber cross section was found to have no effect on the temporal thermal response, which is beneficial for fiber sensing applications. Finally, the simulation results obtained are somewhat different from the experimental data and the possible error sources were analyzed in detail. The simulation results also indicate that the temporal thermal response is inversely proportional to thermal mass of the fiber. The model produced has been validated and could be used to predict the temporal performance of a range of fibers of different diameters (and masses) for various sensor applications.

This research was supported by the Hong Kong Special Administrative Region (SAR) government through a General Research Fund grant PolyU 5296/06E.

References

1. Y. H. Shen, J. Xia, T. Sun, and K. T. V. Grattan, "Photosensitive indium-doped germano-silica fiber for strong FBG with high temperature sustainability," IEEE Photon. Technol. Lett. **16**, 1319–1321 (2004).
2. Y. H. Shen, J. L. He, T. Sun, and K. T. V. Grattan, "High-temperature sustainability of strong fiber Bragg gratings written into Sb-Ge-codoped photosensitive fiber: decay mechanisms involved during annealing," Opt. Lett. **29**, 554–556 (2004).
3. C. W. Smelser, S. J. Mihailov, and D. Grobnic, "Formation of Type I–IR and Type II–IR gratings with an ultrafast IR laser and a phase mask," Opt. Express **13**, 5377–5386 (2005).
4. E. Wikszak, J. Thomas, J. Burghoff, B. Ortac, J. Limpert, and S. Nolte, "Erbium fiber laser based on intracore femtosecond-written fiber Bragg grating," Opt. Lett. **31**, 2390–2392 (2006).
5. M. Bernier, D. Faucher, R. Vallée, A. Saliminia, G. Androz, Y. Sheng, and S. L. Chin, "Bragg gratings photoinduced in ZBLAN fibers by femtosecond pulses at 800 nm," Opt. Lett. **32**, 454–456 (2007).
6. D. Grobnic, S. J. Mihailov, R. B. Walker, C. W. Smelser, C. Lafond, and A. Croteau, "Bragg gratings made with a

femtosecond laser in heavily doped Er-Yb phosphate glass fiber," IEEE Photon. Technol. Lett. **19**, 943–945 (2007).
7. Y. H. Li, C. R. Liao, D. N. Wang, T. Sun, and K. T. V. Grattan, "Study of spectral and annealing properties of fiber Bragg gratings written in H_2-free and H_2-loaded fibers by use of femtosecond laser pulses," Opt. Express **16**, 21239–21247 (2008).
8. A. J. V. Wyk, P. L. Swart, and A. A. Chtcherbakov, "Fiber Bragg grating gas temperature sensor with fast response," Meas. Sci. Technol. **17**, 1113–1117 (2006).
9. C. W. Smelser, S. J. Mihailov, and D. Grobnic, "Hydrogen loading for fiber grating writing with a femtosecond laser and a phase mask," Opt. Lett. **29**, 2127–2129 (2004).
10. D. Grobnic, C. W. Smelser, S. J. Mihailov, and R. B. Walker, "Long-term thermal stability tests at 1000 °C of silica fibre Bragg gratings made with ultrafast laser radiation," Meas. Sci. Technol. **17**, 1009–1013 (2006).
11. G. M. H. Flockhart, R. R. J. Maier, J. S. Barton, W. N. Macpherson, J. D. C. Jones, K. E. Chisholm, L. Zhang, I. Bennion, I. Read, and P. D. Foote, "Quadratic behavior of fiber Bragg grating temperature coefficients," Appl. Opt. **43**, 2744–2751 (2004).
12. T. L. Lowder, J. A. Newman, W. M. Kunzler, J. D. Young, R. H. Selfridge, and S. M. Schultz, "Temporal response of surface-relief fiber Bragg gratings to high temperature CO_2 laser heating," Appl. Opt. **47**, 3568–3573 (2008).
13. S. H. Cho, J. Park, B. Kim, and M. H. Kang, "Fabrication and analysis of chirped fiber Bragg gratings by thermal diffusion," ETRI J. **26**, 371–374 (2004).
14. Y. Wang and K. Vafai, "An experimental investigation of the thermal performance of an asymmetrical flat plate heat pipe," Int. J. Heat Mass Transfer **43**, 2657–2668 (2000).
15. M. Sumetsky, Y. Dulashko, J. M. Fini, A. Hale, and D. J. DiGiovanni, "The microfiber loop resonator: theory, experiment, and application," J. Lightwave Technol. **24**, 242–250 (2006).
16. A. J. C. Grellier, N. K. Zayer, and C. N. Pannell, "Heat tranfer modeling in CO_2 laser processing of optical fibers," Opt. Commun. **152**, 324–328 (1998).
17. G. Rego, L. M. N. B. F. Santos, and B. Schröder, "Estimation of the fiber temperature during an arc-discharge," Microwave Opt. Technol. Lett. **50**, 2020–2025 (2008).